Journal of Oceanography
Vol. 51, pp. 111 to 132. 1995

Wind Relaxation as a Possible Cause of the South China Sea Warm Current

SHENN-YU CHAO[1], PING-TUNG SHAW[2] and JOE WANG[3]

[1]*Horn Point Environmental Laboratories, University of Maryland, Cambridge, Maryland 21613-0775, U.S.A.*
[2]*Department of Marine, Earth and Atmospheric Sciences, North Carolina State University, Raleigh, NC 27695-8208, U.S.A.*
[3]*Institute of Oceanography, National Taiwan University, Taipei, Taiwan*

(Received 9 May 1994; in revised form 25 July 1994; accepted 18 August 1994)

Winter appearance of a northeastward warm current off the southern coast of China against gale force winds is well documented but lacks a plausible explanation. Relaxation of northeasterly winds is envisaged here as a possible cause of the South China Sea Warm Current in winter. A three-dimensional circulation model for the South China Sea is first driven to equilibrium by climatological forcings. Thereafter, wind forcing is relaxed from the 15th day of each month for 9 days. In winterlike months from December to April, the wind relaxation invariably triggers a northeastward current of which the location and alongshore span are comparable to that of the observed warm current. This current is driven by the pressure gradient along the northwestern boundary of the South China Sea, sea level being high to the southwest and low to the northeast. The sea level gradient is built up by the monsoon-driven southwestward coastal current along the northwestern boundary and, after wind relaxes, triggers a return current and a sea level drop that expand southwestward from the southern coast of China to the east coast of Vietnam. The current is initially barotropic, becoming increasingly baroclinic in time as warm waters from the south are advected northeastward. The model also suggests that the sea level gradient is present in most of the months of the year, but is not as dramatic as in winter to trigger fundamental changes in the circulation of the South China Sea.

1. Introduction

The South China Sea Warm Current is a northeastward current over the northern shelf of the South China Sea. The axis of this current is often found between 200 m and 400 m isobaths (Fig. 1). The current is probably originated from the vicinity to the southeast of Hainan Island and reaches as far north as the southern extremity of the Taiwan Strait, spanning an alongshore distance of 600–700 km or more (Guan, 1985). Estimates based on hydrography suggested that the warm current can be as wide as 160–300 km and extends downward to about 300 m from the surface (Guan, 1978). Direct current measurements and geostrophic estimates suggested that the maximum surface speed can be as large as 30 cm/s, carrying a transport of up to 10 Sv northeastward (Guan, 1978). Questions concerning the steadiness of the warm current have not been fully resolved. While the warm current had been documented in almost all months of the year, it is still questionable whether the current is continuous in time. Hydrographies (for example, in March 1967) occasionally did not support the existence of this warm current (Guan,

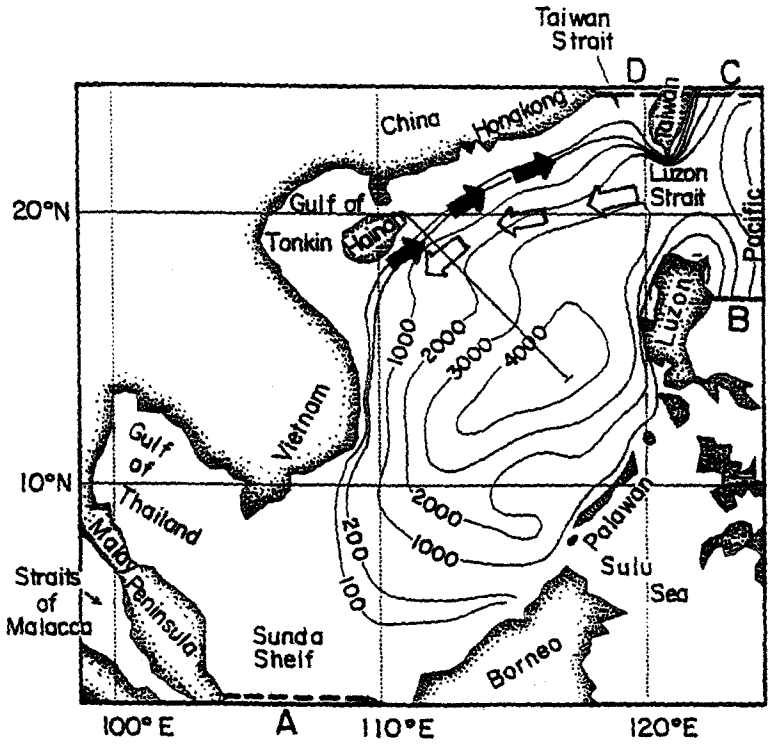

Fig. 1. The map of the South China Sea and the domain of simulation. Bottom topography is shown by the 100, 200, 1000, 2000, 3000 and 4000-m isobaths. Open ocean boundaries are indicated by thick dashed lines (A, B, C and D). The solid and open arrows illustrate schematically the South China Sea Warm Current and Kuroshio intrusion current in winter, respectively. A northwest-southeast transection stretching out from Hainan is used to show vertical features.

1985). Furthermore, there might occasionally be currents alternating in sign inshore and offshore of the warm current (Guan, 1978). Limited hydrographies in 1966–1968 also led to the tentative conclusion that this current intensified in winter (Guan, 1985).

In winterlike months (December–April), there is a southwestward current immediately offshore of the South China Sea Warm Current. In the winters of 1981 and 1982, the depth and width of this current were up to about 800 m and 150 km, respectively, near the northeastern extremity of the South China Sea (117°E, 20°N) (Guo *et al.*, 1985). Concurrent current measurements suggested a maximum surface speed of about 30 cm/s; geostrophic estimates yielded a transport of up to 10 Sv southwestward. The depth, width and strength of this current farther southwestward are not well documented. Water mass analysis (Shaw, 1989, 1991) indicated that the core of this current originated from the Kuroshio intrusion into the South China Sea through the Luzon Strait and diminished in summer months.

Simple mass balance gives clues of how the South China Sea Warm Current ends and how the Kuroshio intrusion current begins in the northeastern reaches of the South China Sea in winter, although this aspect of circulation was never investigated before. The transport in the Taiwan Strait, whether southward or northward, is on the order of 1 Sv. Across the Luzon Strait, monthly mean transports are 3–4 Sv into the South China Sea in winter (Wyrtki, 1961). If the

South China Sea Warm Current carries a transport much beyond 1 Sv, it must turn anticyclonically and back into the South China Sea near the southern end of the Taiwan Strait, hopefully entraining into the southwestward Kuroshio intrusion current. Should the latter transpire, then the transport of the Kuroshio intrusion current will increase downstream of the Luzon Strait, explaining why the geostrophic estimate (up to 10 Sv) made by Guo *et al.* (1985) inside the South China Sea far exceeds the climatological mean transport through the Luzon Strait.

The major circulation in the South China Sea is driven by the monsoon winds (Wyrtki, 1961). The annual cycle of the mean wind stress field (Hellerman and Rosenstein, 1983) is illustrated in Fig. 2. Winds prior to September are dominated by the southwest monsoon. In September, the northeast monsoon begins to appear in the seas north of 20°N. South of that latitude, the southwest monsoon still prevails. The northeast monsoon expands southward against the diminishing southwest monsoon in October, reaching its maximum strength and covering the entire South China Sea in December. April marks the end of the winter monsoon. The southwest monsoon first appears in the central basin in May and expands over the entire basin in July and August.

The southwest monsoon makes the appearance of the South China Sea Warm Current dynamically possible from May to August. In winterlike months, especially from December to April, the appearance of the warm current against the local northeasterly winds of 0.2 Pa mean strength is counterintuitive. Wyrtki's (1961) climatological atlas did not contain such a warm current in winter, neither did the mean ship drift data with 1-degree resolution (Levitus, 1982). All existing models have successfully reproduced the Kuroshio intrusion current but not the South China Sea Warm Current in winter. Barotropic models driven by climatological mean

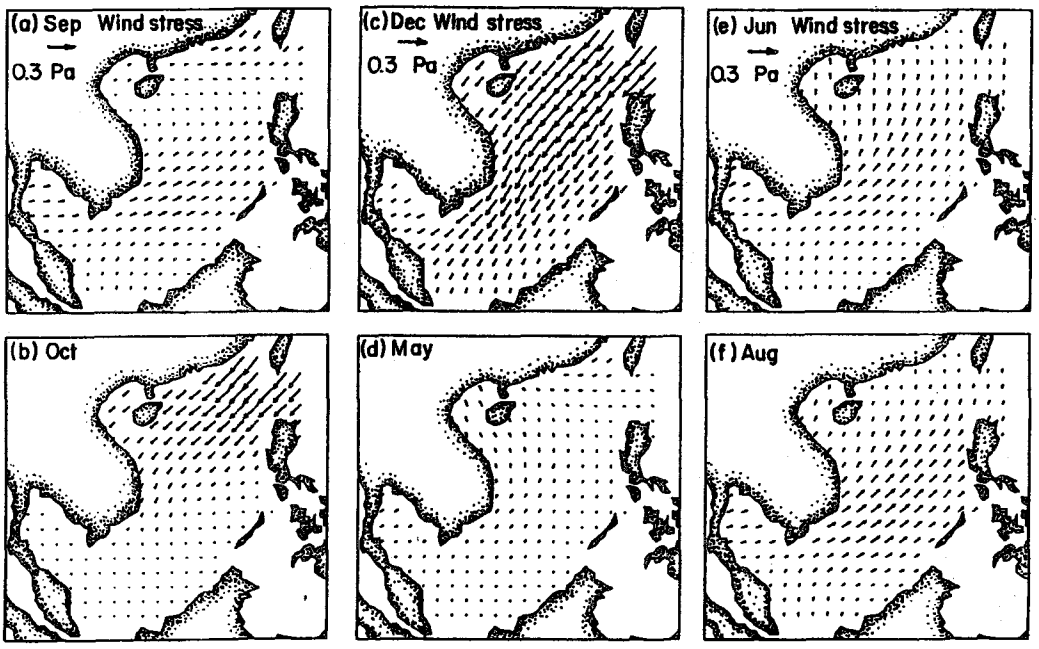

Fig. 2. Wind stress distributions from Hellerman and Rosenstein (1983). Months are chosen to show the development of winter and summer monsoons, (a) September, (b) October, (c) December, (d) May, (e) June, and (f) August. Calibration arrows are 0.3 Pa for all plots.

winds failed to reproduce the warm current in winter (Li *et al.*, 1992; Zeng *et al.*, 1989). The winter appearance of this warm current is also conspicuously absent in 3-D models that include baroclinicity and a free surface (Pohlmann, 1987; Shaw and Chao, 1994). In consequence, the dynamical origin of the South China Sea Warm Current has yet to be identified.

The northeast monsoon, being a southward extension of westerlies, is of squally type, each episode lasting a few days. Thus, ocean models driven by monthly mean winds produce mean currents of some sort but suppress transients. Unlike major currents such as Kuroshio, the signal (driven by the mean winds) to noise (driven by transients) ratio associated with monsoon-driven currents is not large. This motivated us to seek transient forcing as a possible generating mechanism for the South China Sea Warm Current.

A rare observational effort (Guo and Huang, 1983) captured interesting features concerning the response of the South China Sea Warm Current to the winter cold air outbreaks south of China. From February 22 to February 26 in 1982, two consecutive cold fronts invaded southward from the China continent. Along the southern coast of China, winds were weak and southwesterly before the cold air arrival, became strong and northeasterly during the cold events, and eventually subsided to weak easterly winds after the passage of fronts. A current meter was deployed at 10 m depth near the core of the Warm Current off a coastal station between Hongkong and Taiwan (116°50′ E, 23°10′ N). The prefrontal current was characteristically northeastward. Northeasterly winds during cold event caused the current to turn counterclockwise. Postfront wind relaxation caused the current to turn clockwise and return to the northeastward direction. Although currents at 10 m depth are greatly influenced by the wind-induced Ekman drift, Guo and Huang's observation suggested that northeastward Warm Current weakened during strong northeasterly winds and rebounded after wind relaxation.

The subject matter is investigated using a 3-D primitive-equation model with a free surface. The South China Sea circulation as inferred from the climatological forcings and boundary conditions was reported earlier (Shaw and Chao, 1994); only relevant features will be reiterated. Climatological forcings at the ocean surface are relaxed for 9 days from the 15th day of each month for the purpose of simulating the South China Sea Warm Current. Since wind forcing changes at the beginning of each month, circulation on the 15th day of each month is more representative of the mean monthly condition. Our results are more than encouraging. In particular, wind relaxation proves to be conducive to the generation of the South China Sea Warm Current. The degree of conduciveness varies from month to month, helping to identify the underlying generating mechanism.

2. Model Description

The model, as described in Shaw and Chao (1994), solves the three-dimensional equations of momentum, continuity, temperature and salinity with Boussinesq and hydrostatic approximations. The model domain as shown in Fig. 1 is from 2°N to 24°N and from 99°E to 124°E with a horizontal resolution of 0.4°. With 21 layers in the vertical, variables are evaluated at the center of each layer at 2.5, 10, 20, 30, 50, 75, 100, 125, 150, 200, 300, 500, 700, 900, 1200, 1500, 2000, 2500, 3000, 4000 and 5000 m. There are four open boundaries in the model, marked by thick dashed lines (A, B, C and D) in Fig. 1. Transport through A and D account for inflow/outflow across 2°N and through the Taiwan Strait, respectively, whereas transports through B and C account for the Kuroshio inflow and outflow. Several narrow and shallow passages to the Sulu Sea are closed because they are too narrow to be resolved by the present model, and because transports through them are quite small. Further, water mass dissimilarity between the South

Table 1. Bimonthly transports (in 10^6 m^3s^{-1}) estimated from Wyrtki (1961) across the open boundaries shown in Fig. 1. These values are sightly adjusted to compensate for the closing of the narrow passages to the Sulu Sea. Positive and negative values represent inflow and outflow, respectively.

Month	Open Boundaries			
	A	B	C	D
January–February	–3.0	27.0	–24.5	0.5
March–April	0	37.5	–37.5	0
May–June	3.0	32.0	–34.0	–1.0
July–August	3.0	28.0	–30.5	–0.5
September–October	–1.0	27.5	–27.0	0.5
November–December	–3.5	24.5	–21.5	0.5

China Sea and Sulu Sea also points out their insignificance. Table 1, derived from Wyrtki (1961), shows bimonthly transport estimates across the four open boundaries.

The model is initialized by January temperature and salinity fields (Levitus, 1982), and is subsequently driven by climatological forcings for 3 years. Monthly mean wind stress field (Hellerman and Rosenstein, 1983) is applied to the ocean surface, while monthly sea surface temperature and salinity are fixed at climatological values provided by Levitus (1982). Radiation boundary conditions are generally employed on open boundaries, except the transports across open boundaries are fixed at Wyrtki's bimonthly estimates. The vertically averaged velocities are therefore fixed on open boundaries, while deviations from the vertical averages are extrapolated from the nearest interior points adjacent to these boundaries. For inflows, waters entering the basin are given the right temperature and salinity according to Levitus' climatological atlas. All the climatological data have one-degree resolution, which obviously limits the amount of baroclinicity to be developed in the model, because typical fronts have much finer horizontal scales.

Coefficients of vertical viscosity and diffusivity are calculated from the Richardson number according to the formulation of Pacanowski and Philander (1981). Horizontally, the mixing coefficient is 5×10^3 m^2s^{-1} for the momentum, temperature and salinity equations. A quadratic stress law is applied at the bottom with a dimensionless drag coefficient of 0. 001.

The total heat content and total kinetic energy of the basin reach steady annual cycles after two years of integration, justifying the use of third year result as climatological mean condition for the wind relaxation experiment. From the 15th day of each month, surface forcings are relaxed for nine days by requiring wind stress to vanish and by replacing fixed sea surface temperature and salinity with no-flux conditions,

$$\frac{\partial}{\partial z}(T,S) = 0 \quad \text{on the ocean surface}$$

where z is the vertical coordinate, T is the temperature and S is the salinity. The relaxation of thermohaline forcing turns out to be inconsequential; almost the entire flow changes in 9 days are caused by wind relaxation.

3. Relaxation of NE Monsoon

Figure 3 shows flow fields at 50 m depth before wind relaxation (upper left), and after wind relaxation at 3-day intervals (remaining 3 panels) in January. The 50 m depth is chosen because it is the most representative of upper ocean circulation. Currents are dominated by Ekman dynamics above 50 m, and attenuate with depths below it. Before the relaxation, the Kuroshio Intrusion Current entering the Luzon Strait accelerates along the northern and western boundaries of the basin in response to the NE monsoon. The southward current off the coast of Vietnam turns cyclonically as it impinges onto the Sunda shelf between 4°N and 6°N. A two-layer circulation develops in the shallow Gulf of Thailand; waters flowing out of the Gulf at 50 m is replenished by a surface inflow. The two layers of circulation, each about 25 m thick, are mostly wind-driven. Northeasterly winds drive an upchannel Ekman drift near the surface which piles up water in the upper reaches of the Gulf. The consequent along-channel pressure gradient drives a return flow at depths. More details were given in Shaw and Chao (1994). The subtidal two-layer circulation in the Gulf, so prominent in the numerical model, has unfortunately yet to be verified observationally in this underexplored area.

Three days after the relaxation, a northeastward current develops along the northwestern shelf of the basin. This current, originating from about 14°N off the coast of Vietnam, hugs the east coast of Hainan along its track northeastward. The location, width and alongshore span of this current fit the description of the South China Sea Warm Current. Concurrent with the appearance of this warm current is a southwestward current moving offshore on the western side of the basin. The absence of NE monsoon wind allows the southward current off Vietnam to turn cyclonically at higher latitudes. Six and nine days after the relaxation, the modeled northeastward warm current shows little sign of weakening, but the remaining currents in the central basin decay continuously and become less organized. It is also seen that the northeastward warm current turns anticyclonically near the southern end of the Taiwan Strait, feeding the southwestward flowing Kuroshio intrusion current.

Snapshots at smaller time intervals (not shown) indicate that the emergence of the northeastward current begins from its northeastern (downstream) extreme (115°E, 21°N) after about 0.75 days of relaxation, and expands southwestward at a speed of about 300 km per day while strengthening. The current becomes fully developed after three days of relaxation. The southwestward expansion is consistent with the propagation direction of continental shelf waves, while the speed of alongshore expansion falls in the range of phase speeds associated with barotropic continental shelf waves in the longwave limit. Off the southern coast of China, the mean water depth increases from 100 m to 3600 m over a cross-shelf distance of 200 km. Assuming the topographic profile is exponential, the phase speed for the longest continental shelf wave is about 310 km per day following Buchwald and Adams (1968).

Figure 4 shows the corresponding sea level fields before wind relaxation (upper left), and after wind relaxation at 3-day intervals (remaining 3 panels) in January. Driven by the NE monsoon, the sea level prior to relaxation is high to the west and low to the east. Not so visibly apparent is the sea level gradient along the northwestern boundary of the basin. Prior to the relaxation, the sea level is about 10 cm off the Vietnam coast at 12°N and –3 cm at Hongkong. Both stations are marked by "×" in the top left panel of Fig. 4. The difference between the two (13 cm) will prove to be a useful prognostic index for the occurrence of the modeled northeastward current during wind relaxation in winter. During the first three days of relaxation, sea level along the southern coast of China drops dramatically. As in the development of the northeastward warm

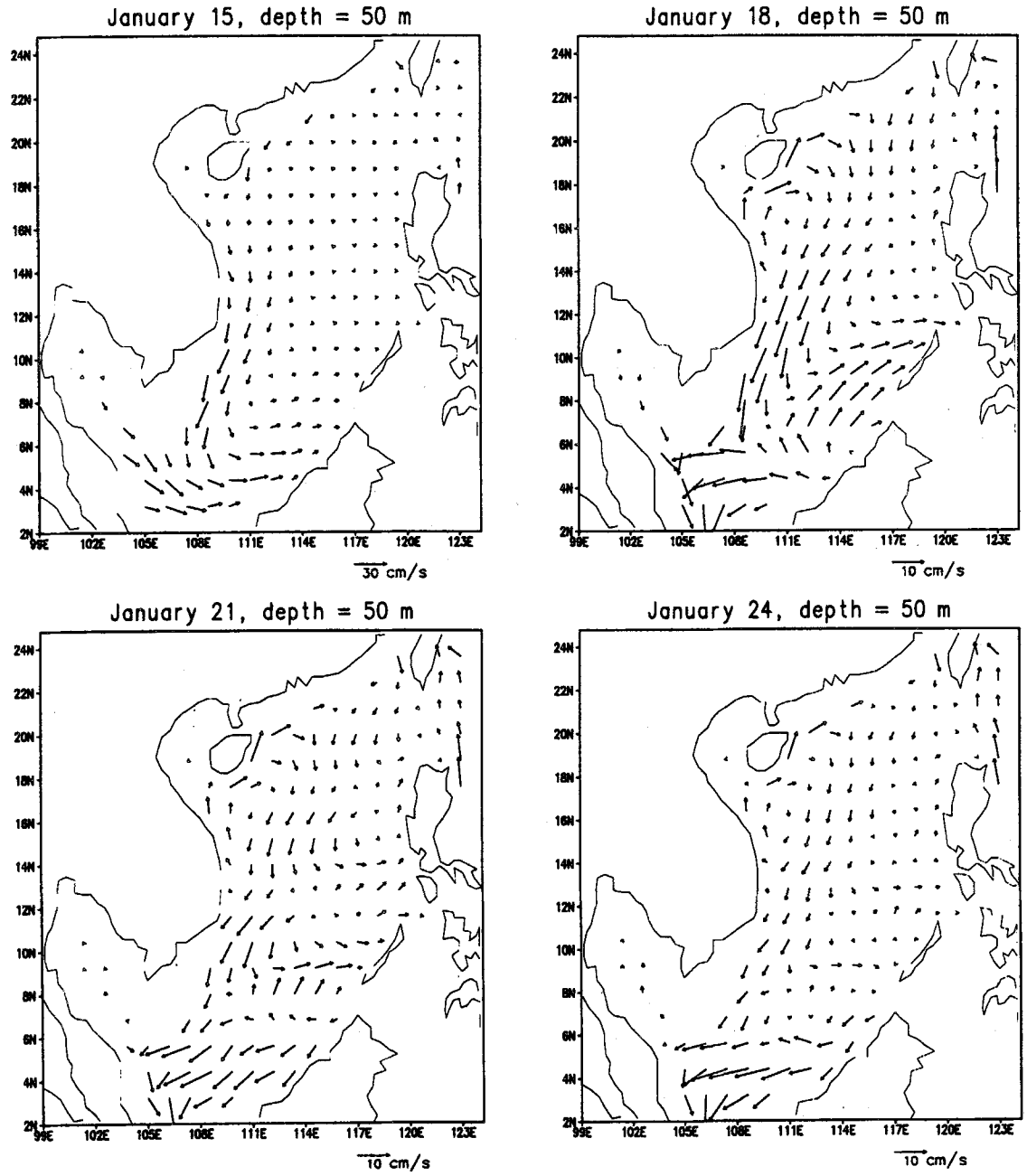

Fig. 3. Flow fields at 50 m depth before wind relaxation on January 15, and after relaxation at 3-day intervals.

current, the coastal sea level drop expands southwestward toward Vietnam in the first three days. Thereafter, the sea level slope from the coast of Vietnam (~14°N) to Hongkong remains relatively unattenuated, capable of sustaining the northeastward warm current.

Figure 5 shows the sea surface temperature prior to and nine days after the relaxation in

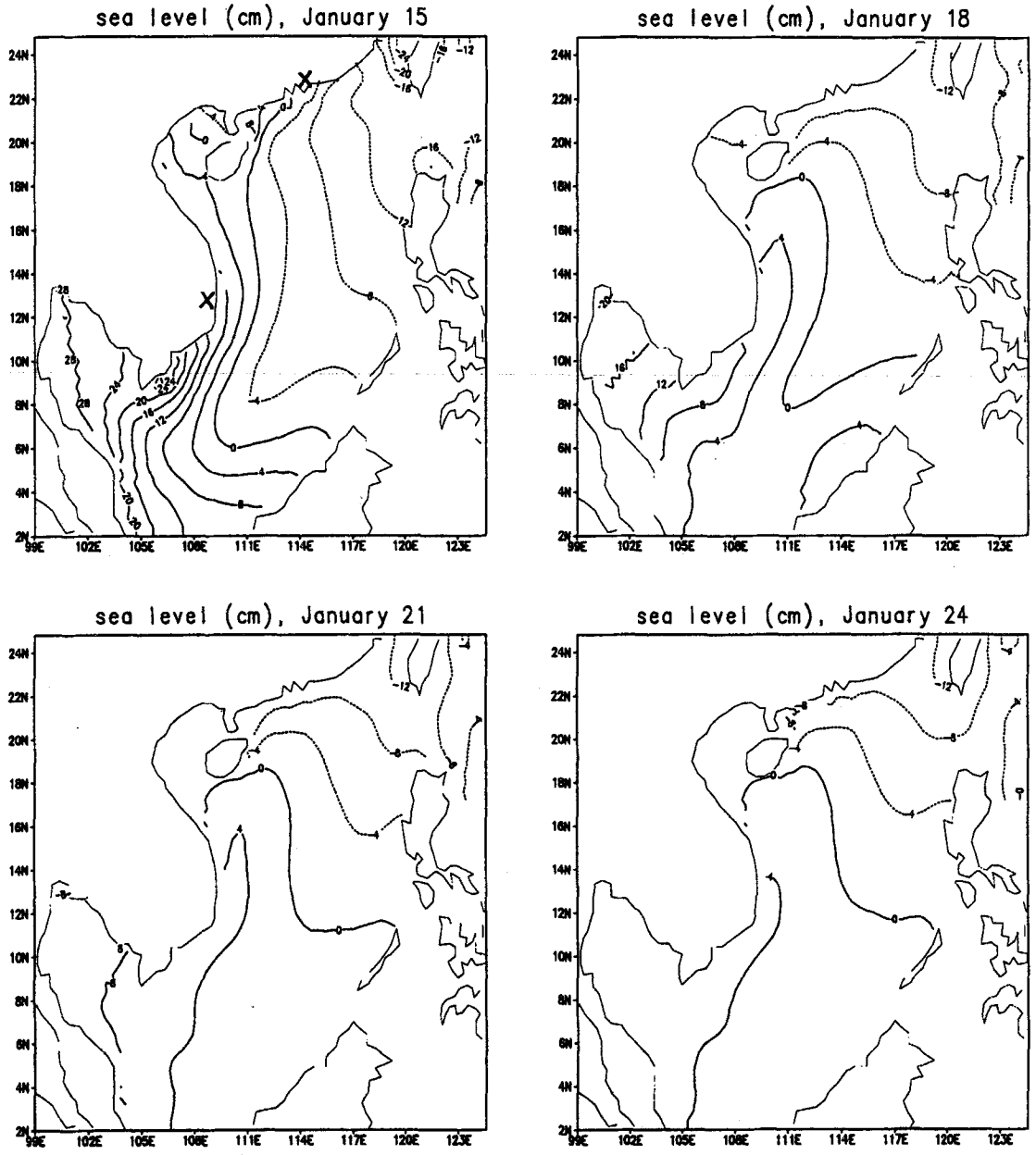

Fig. 4. Sea level fields (in cm) before wind relaxation on January 15, and after relaxation at 3-day intervals. Dotted contours are below mean sea level. Two coastal stations marked by "×" in the top left panel will be used to define a sea level index later.

January. Changes brought about by relaxation are relatively small. Nowhere is seen persistent upwelling that substantially changes the sea surface temperature. Displacement due to horizontal advection is generally insignificant, comparable to the horizontal grid spacings of the model over nine days of relaxation.

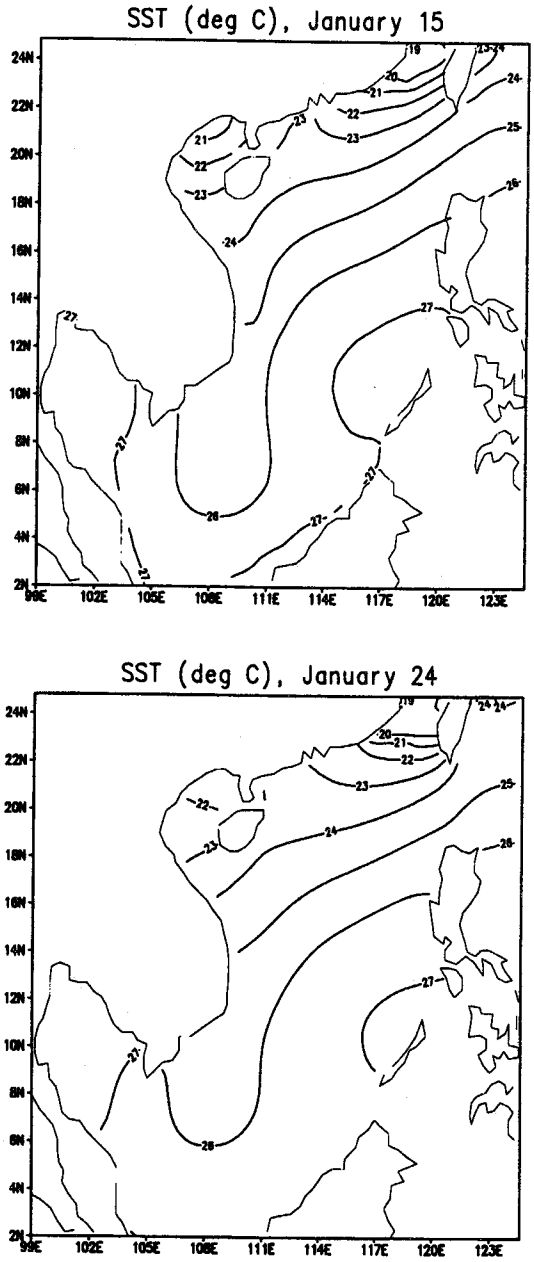

Fig. 5. Sea surface temperature (in °C) before wind relaxation on January 15, and nine days after wind relaxation on January 24.

4. Relaxation of SW Monsoon

As the SW monsoon appears over the South China Sea in May and June, the condition may be favorable for the development of the South China Sea Warm Current even without wind relaxation. Since responses in both months are similar, only May experiment is discussed below. In Fig. 6, the left two panels show flow fields at 50 m depth prior to and three days after the wind

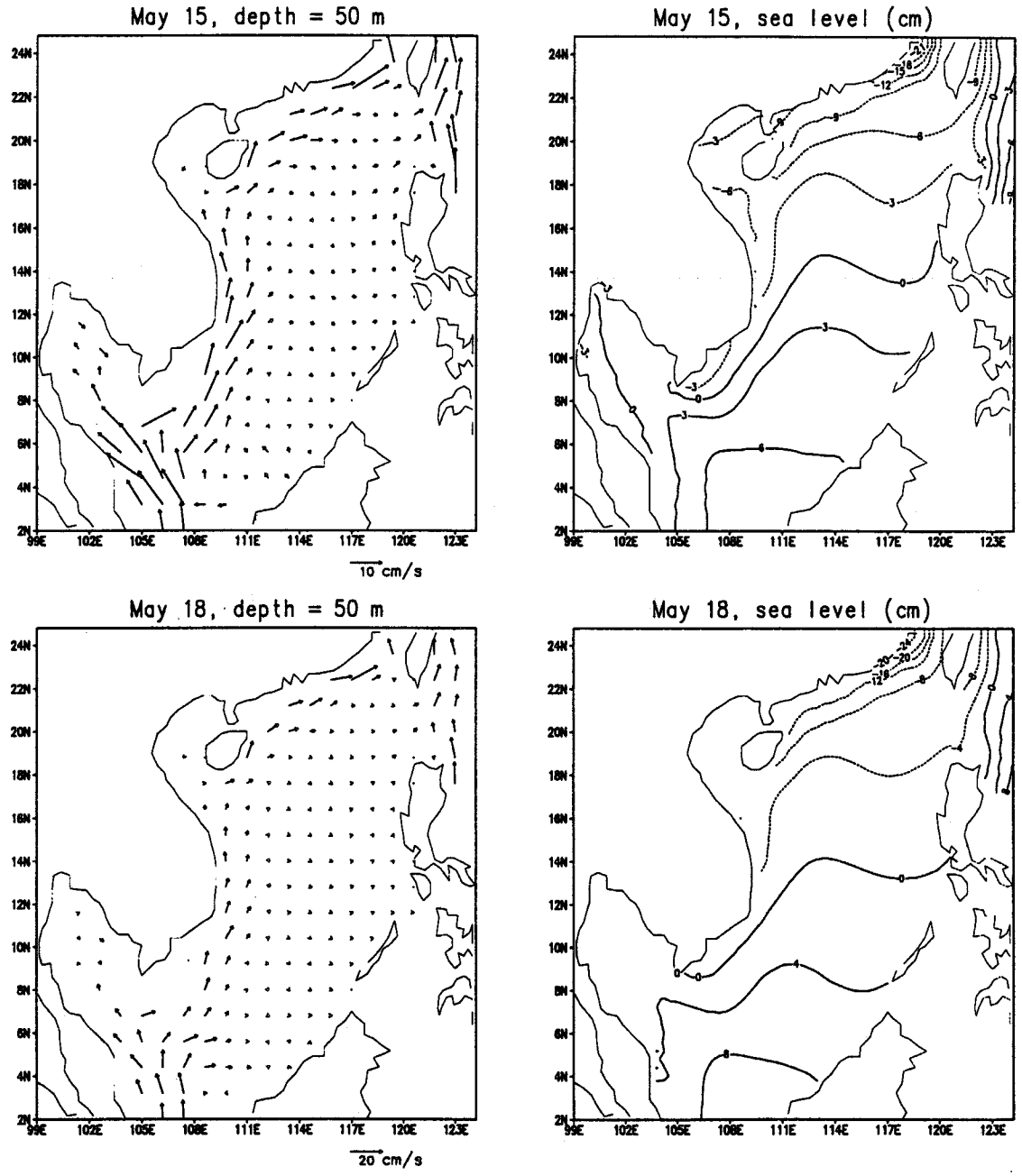

Fig. 6. Flow fields at 50 m depth (left panels) and sea level fields in centimeters (right panels) prior to wind relaxation on May 15 (top) and 3 days after relaxation (bottom). Dotted sea level contours are below mean sea level.

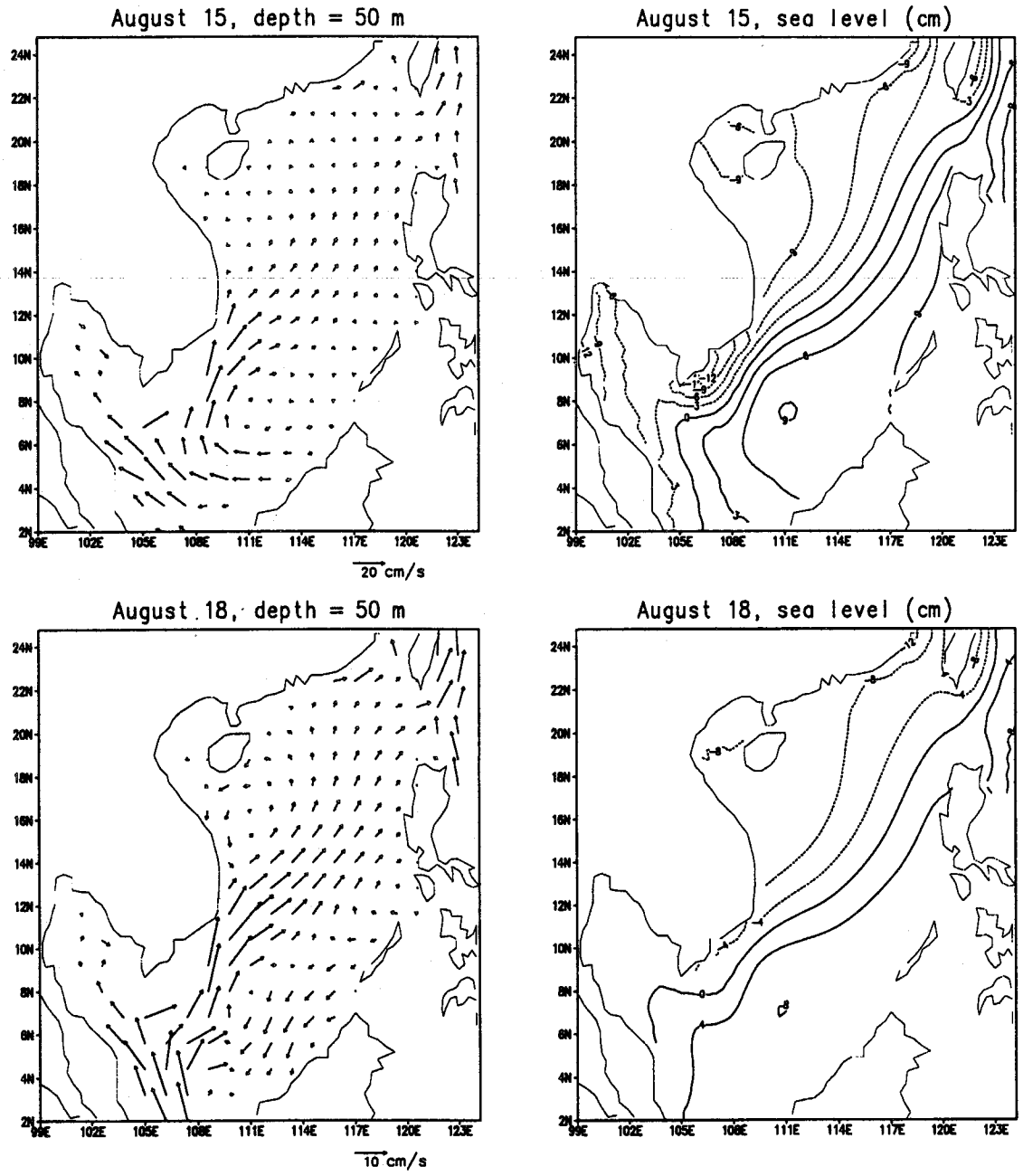

Fig. 7. As in Fig. 6 except for August relaxation experiment.

relaxation, whereas the right two panels show corresponding sea level distributions. In this first month of the SW monsoon, the northeastward coastal jet is continuous along the western and northern boundaries of the basin. The two-layer circulation in the Gulf of Thailand is reversed; flow entering the Gulf at 50 m depth returns near the surface. The sea level field, being high to the south and low to the north, shows little sign of letting up after three days of relaxation, neither does the flow field. These patterns remain relatively unattenuated even after 9 days of wind relaxation.

The summerlike circulation becomes fully developed in July and August. Since the patterns prior to and after relaxation are similar in these two months, only the August result is shown below. Figure 7 shows flow fields at 50 m depth and sea level fields before and three days after relaxation in August. Prior to relaxation, the northward coastal jet off the southern Vietnam separates from the coast and flows northeastward toward the Luzon Strait. This jet separation was envisioned earlier by Wyrtki (1961). Remnants of northeastward current in the northern reaches of the basin are mostly absent. Subsequent wind relaxation intensifies a cyclonic eddy to the south of Hainan. The two-layer circulation of the Gulf of Thailand in summer reaches its maximum strength in July and August.

The July–August intensification of the recirculation eddy south of Hainan triggered by wind relaxation is made possible by the much weakened meridional pressure gradient in that region. Comparing the August sea level with that in May, it is clear that the stronger sea level slope south of Hainan in May acts to suppress the development of a recirculation eddy.

5. Wind Relaxation during Fall Transition

In September–November, the transition period from the SW monsoon to NE monsoon, our wind relaxation experiments fail to produce the northeastward warm current. This negative result should be put in proper perspective, as the South China Sea Warm Current had been observed in all these three months. What should be concluded from the negative result is that the mean condition derived from climatological forcings is less favorable for the development of the warm current during wind relaxation from September to November. As the real condition in the South China Sea may differ from the multi-year average substantially, and realistic wind forcing may relax many times in one month, wind relaxation as a possible cause of the South China Sea Warm Current cannot be dismissed in these three months.

A comparison between November and December responses sheds light to the generating mechanism of the warm current. Figure 8 shows flow fields at 50 m depth and sea level distributions before and three days after relaxation in November, whereas the corresponding responses in December are shown in Fig. 9. Prior to wind relaxation, the flow fields in these two months are almost indistinguishable. The relaxation-induced northeastward warm current is sizeable in December but barely noticeable in November. Sea level gradients along the northwestern boundary of the basin differ between these two months. The sea level difference between the coast of Vietnam at 12°N and Hongkong serves as a useful index to quantify the difference. Sea level off the coast of Vietnam at 12°N is higher than Hongkong sea level by about 5 cm in November and by about 10 cm in December. The piling up of waters to the south due to the southward coastal current along the northwestern boundary of the basin continues unabatedly from October to January. The sea level gradient is not enough to trigger a northeastward warm current during wind relaxation in November, but is able to trigger and sustain the reverse current during nine days of wind relaxation in December.

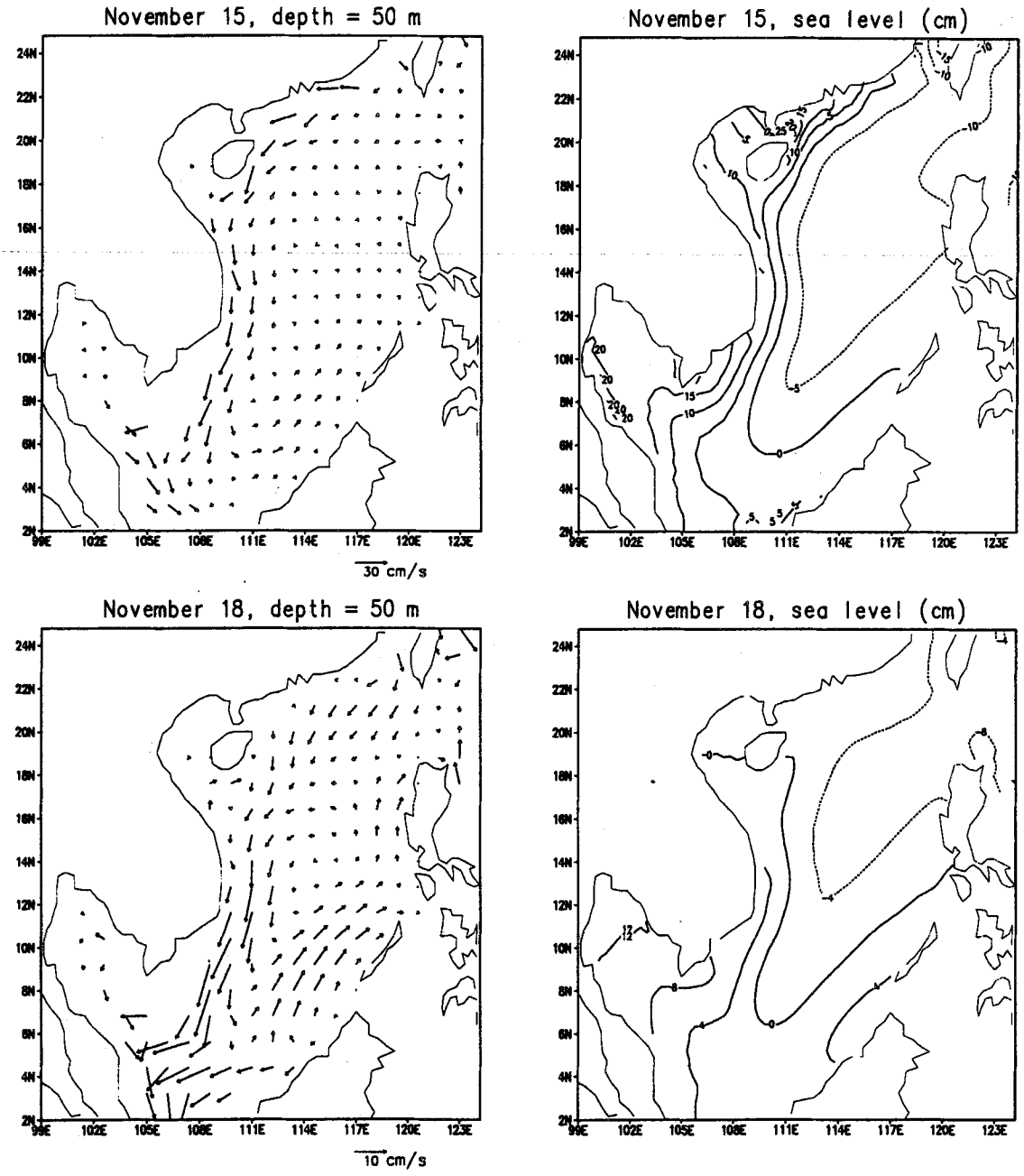

Fig. 8. As in Fig. 6 except for November relaxation experiment.

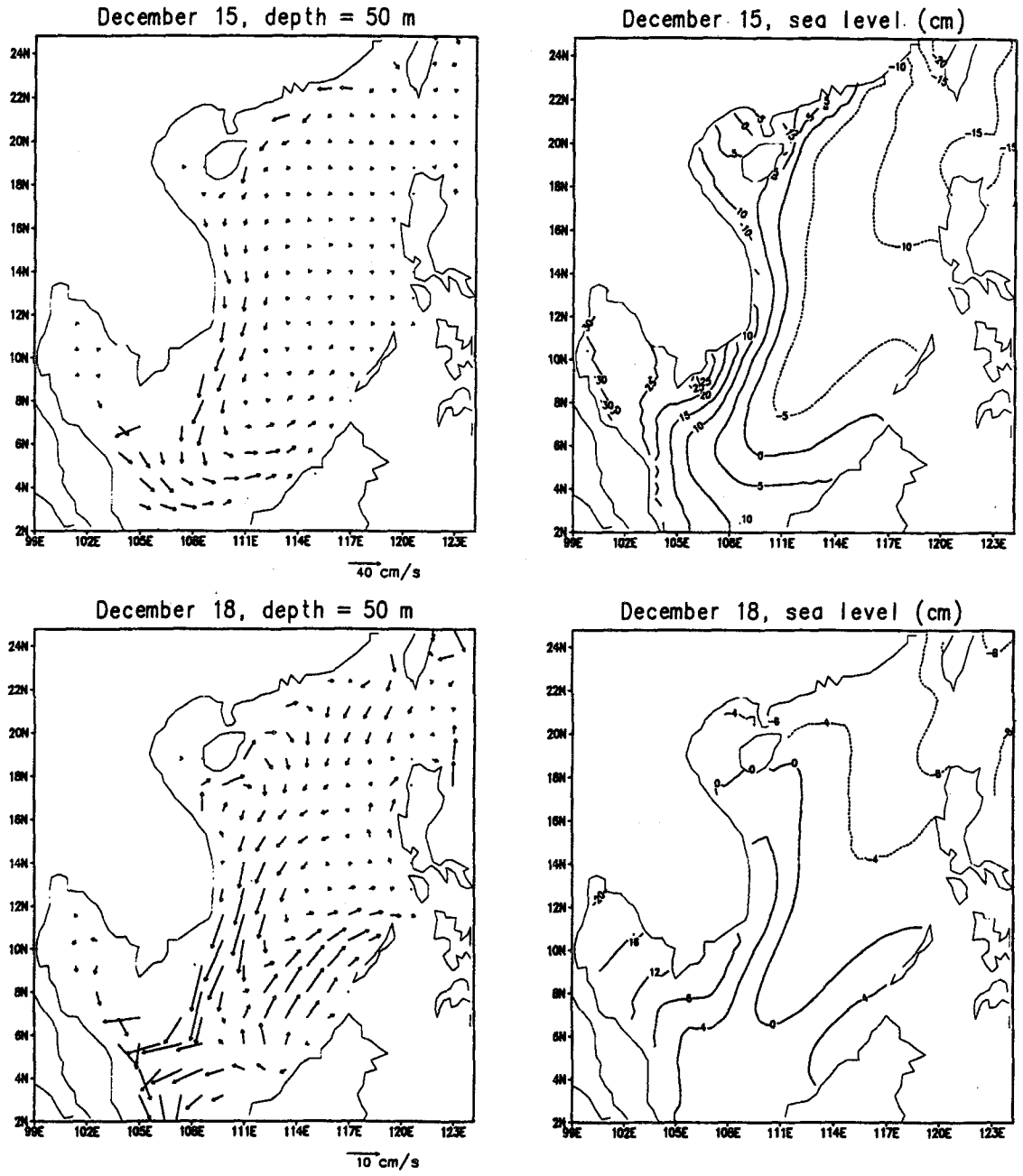

Fig. 9. As in Fig. 6 except for December relaxation experiment.

6. A Prognostic Sea Level Index

Figure 10 shows the estimated sea level differences between the coast of Vietnam at 12°N and Hongkong on the 15th day of each month before the wind is relaxed. The two stations (marked by "×" in the top left panel of Fig. 4) are chosen to cover the entire alongshore span of the northeastward warm current generated by wind relaxation in winter. During most times of a year, our climatology-driven model suggests that sea level is higher to the south along northwestern boundary of the basin. The difference increases from October to January with the aid of NE monsoon, and decreases thereafter as the diminishing NE monsoon is gradually replaced by the SW monsoon. From September to October, the reappearance of NE monsoon over northern reaches of the basin builds up a band of high sea level along the northern boundary, reversing the sea surface slope along the northwestern boundary of the basin.

The sea level index correlates well with subsequent development of the northeastward warm current after wind relaxation. From December to April, the large and positive indices are able to trigger the northeastward warm current after the relaxation of NE monsoon. From May to June, the northeastward current is initially maintained by the SW monsoon and after wind relaxes, is sustained by the sea surface slope as indicated by the modest and positive sea level indices. In July and August, sea level indices are quite small and our climatology-driven model does not produce the northeastward warm current whether the wind is relaxed or not. The model-produced

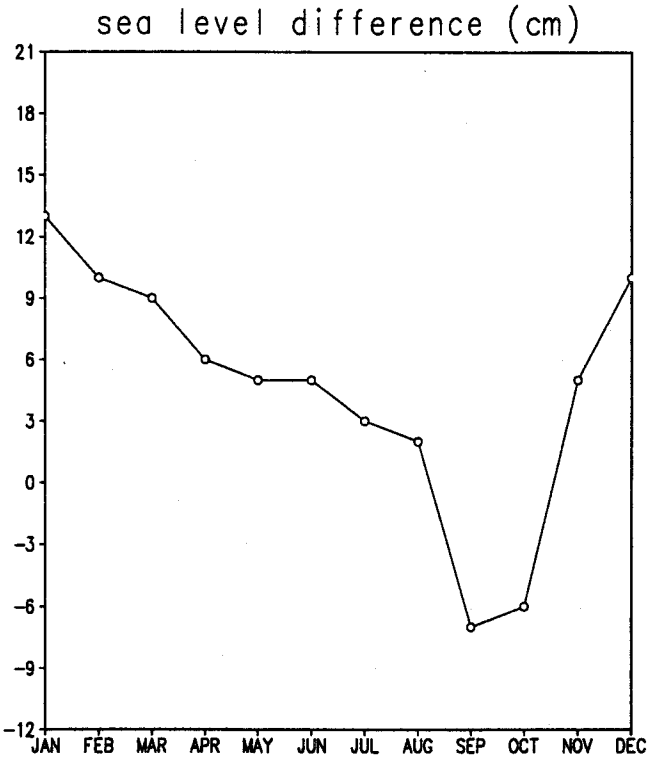

Fig. 10. Model-estimated sea level difference (cm) between the coast of Vietnam at 12°N and Hongkong on the 15th day of each month before wind relaxation. Positive values indicate higher sea levels to the south.

sea level indices are negative in September and October, unable to trigger the northeastward warm current during wind relaxation. The sea level index begins to rebound to a positive value (5 cm) in November, but falls short of producing a sizeable reverse coastal current against the ambient southwestward current after the wind relaxes.

7. Boundary Forcing Relaxation

When wind forcing is relaxed, it is not clear how inflows and outflows through open boundaries should be adjusted in a dynamically consistent manner. The answer depends on how much of inflow/outflow fluctuations are driven by winds over the South China Sea and how much are remotely driven. The foregoing simulations assume all inflows and outflows are remotely forced and therefore remain constant when winds over the South China Sea are relaxed. The other extreme, that all inflows and outflows other than the Kuroshio are locally forced by winds over the South China Sea, is examined below. Under this scenario, flows entering and leaving the South China Sea are required to vanish in conjunction with wind relaxation.

January relaxation experiment is repeated below except with the addition of boundary forcing relaxation. In January, transport estimates based on Wyrtki's climatological atlas (Table 1) contain 2.5 Sv of Kuroshio inflow from the Luzon Strait, 0.5 Sv of inflow from the Taiwan Strait, and 3 Sv of outflow leaving the Sunda Shelf from between Borneo and Malay Peninsula. These transports are set to zero while an equal amount of inflow and outflow of 27 Sv for the Kuroshio east of Luzon Strait is used. Concerns about the basinwide volume conservation forbid us to close each opening individually.

Figure 11 shows flow fields at 50 m depth before (upper left) and after the relaxation event at 3-day intervals (remaining 3 panels) in January. The similarities between Fig. 3 and Fig. 11 are striking, suggesting that boundary forcing relaxation is not nearly as important as wind relaxation in changing the flow pattern. More quantitatively, boundary forcing relaxation strengthens the northeastward transport of the warm current by about 50 percent. More details are given in the next section. Conceivably, this is caused by the relaxation of boundary forcings from the Taiwan and Luzon Straits, as disturbances should be transmitted in the direction bounded to the right by the coastline. The relaxation of boundary forcing at 2°N reduces southward flows over the Sunda shelf below 4°N and, as disturbances propagate in the right-bounded direction, enhances the northeastward flow to the west of Palawan. Overall, changes brought about by boundary forcing relaxation are too minor to upset the basinwide circulation pattern.

The effect of boundary forcing relaxation in other months ranges from minor (as in January) to negligible. These cases are not discussed here for brevity.

8. Vertical Features

Vertical features of the northeastward warm current and its relation to the offshore currents in winter are examined here, using January relaxation experiments as examples. A NW-SE transection is chosen, stretching out from the northeastmost corner of the Hainan Island (see Fig. 1). Figure 12 shows the vertical section of alongshore (NE-SW) currents three days after both the wind and boundary forcing are relaxed. The plane view of flows corresponding to this section was shown in the upper right panel of Fig. 11. The fresh northeastward current is confined to within 180 km from Hainan coast, extends vertically to a depth less than 200 m, and contains a strong barotropic component. The opposite (southwestward) current offshore is wider (~600 km) and deeper (~350 m). The northeastward coastal current remains relatively unattenuated for six

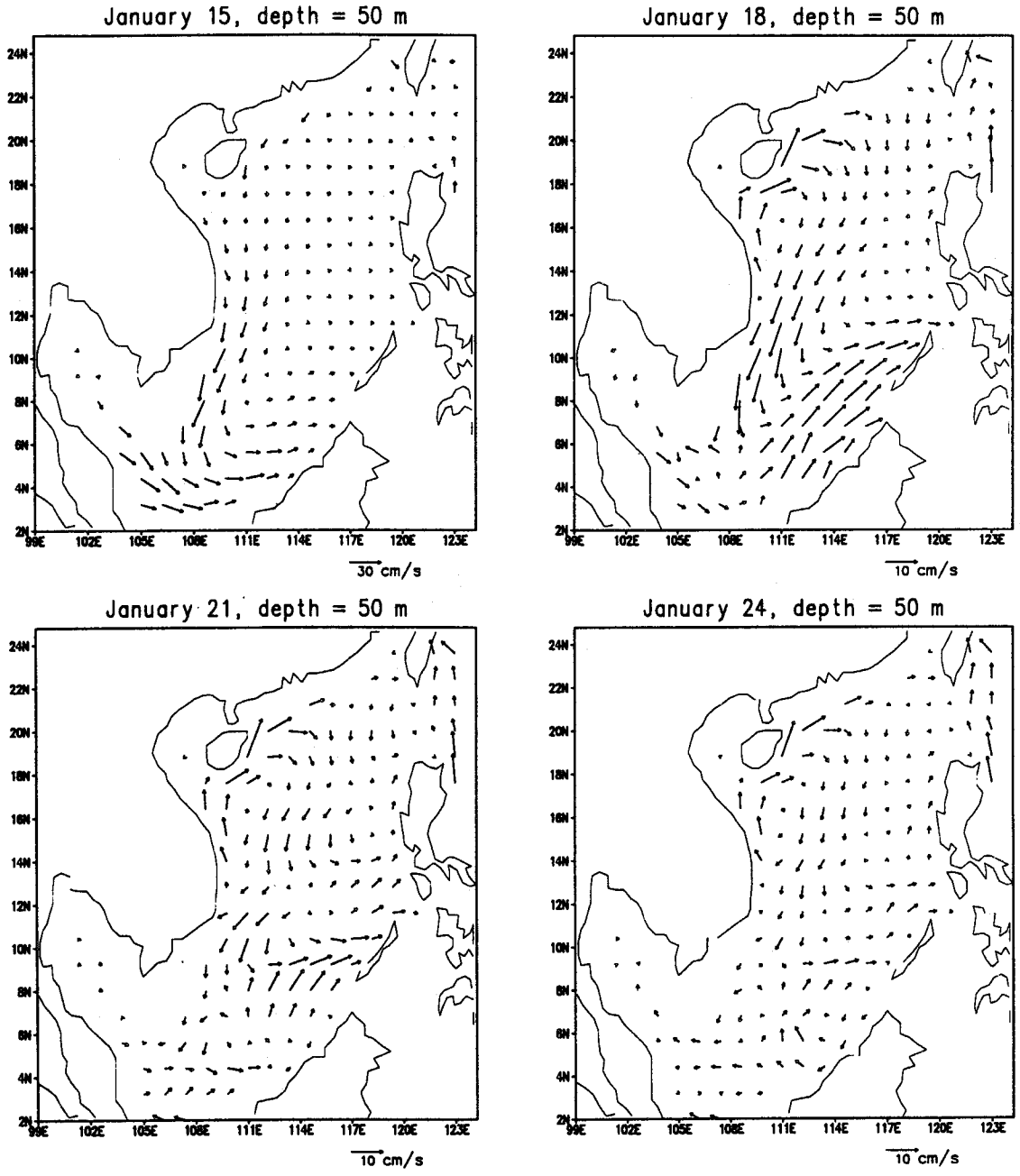

Fig. 11. As in Fig. 3 except inflows and outflows other than the Kuroshio are relaxed simultaneously with the wind relaxation.

more days of relaxation. Transport estimates from this and several other cross-shelf sections suggest that this current carries 1~1.5 Sv northeastward if only wind forcing is relaxed, and about 1.5~2 Sv northeastward if inflows and outflows are relaxed simultaneously. These values are clearly below some of the observation-based estimates.

Being initially barotropic, the presence of the northeastward coastal current is not well reflected in temperature sections. The desired baroclinic signature in temperature sections is likely to require time, after sufficient amount of warm water from the south is carried northeastward by this current. Indeed, isotherm slope becomes increasingly visible during the nine-day relaxation. For this reason, a temperature section after nine days of relaxation is shown

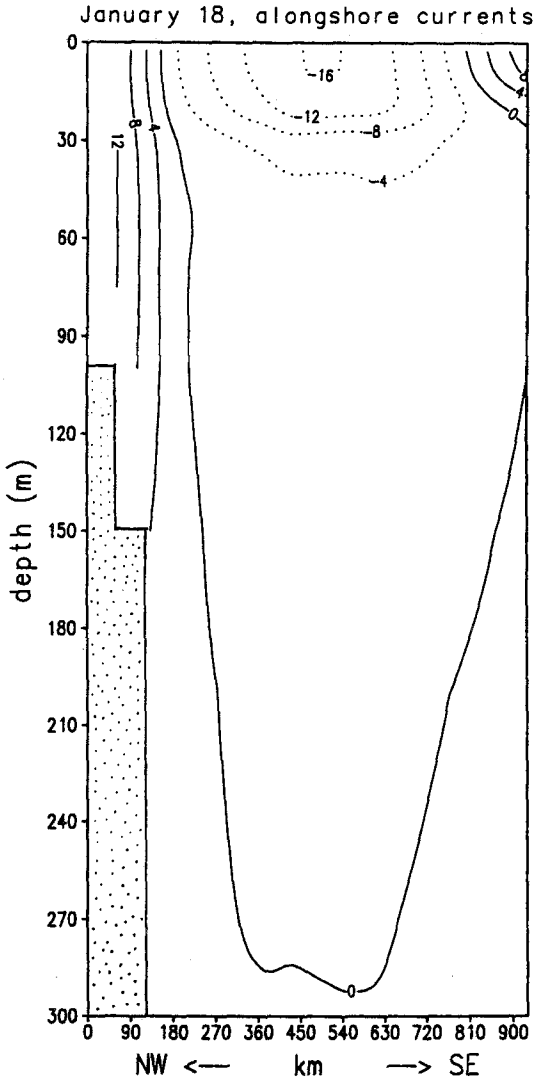

Fig. 12. Vertical section of alongshore currents in cm/s three days after the wind and boundary forcing are relaxed simultaneously in January (see text). The section is NW-SE, stretching out southeastward from the northeasternmost corner of Hainan. Solid and dotted contours represent northeastward and southwestward currents, respectively.

in Fig. 13 to accentuate the response. The vertical section corresponds to the case in which both wind and boundary forcing are relaxed simultaneously. If only the wind forcing is relaxed, the consequent northeastward current is weaker; the development of isotherm slope will be similar but slightly slower.

It is seen in Fig. 13 that isotherms first deepens in the seaward (southeastward) direction in response to the northeastward coastal current, and then rises in response to the southwestward offshore current. The observed isotherms (Guan, 1978) showed similar but steeper slopes. The modest amount of baroclinicity suggested by observations is inadequately reproduced by the model, partly because one relaxation event is too short to establish baroclinicity. More discussion on this will be given below. The isotherm slope associated with the northeastward coastal current is confined to the upper ocean, becoming much less discernible at depths below 200 m.

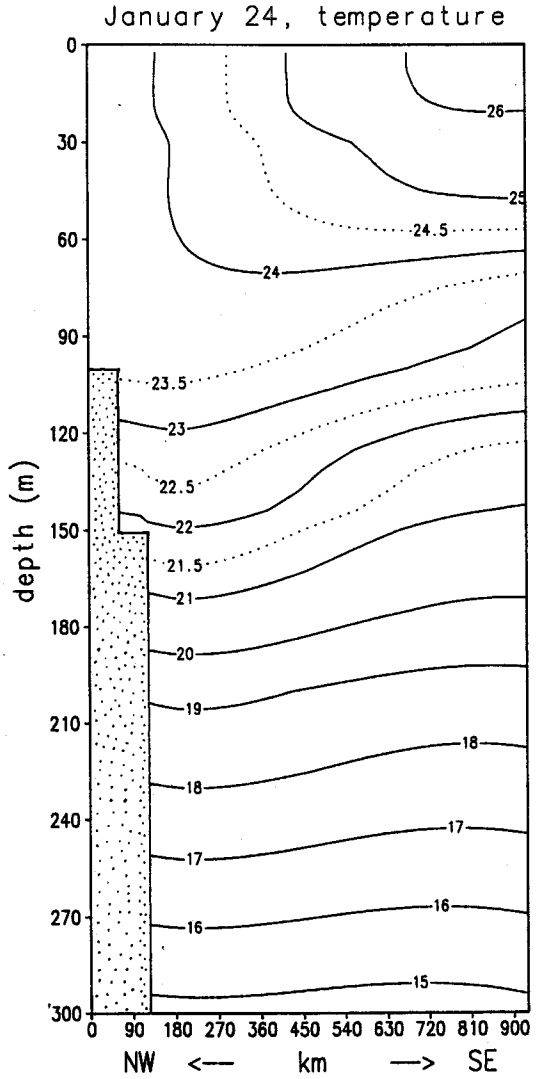

Fig. 13. Temperature section (in °C) nine days after wind and boundary forcings are relaxed simultaneously in January (see text). The NW-SE section is the same as in Fig. 12.

9. Discussion and Conclusions

Wind relaxation as a possible cause of the South China Sea Warm Current is envisaged here using a three-dimensional primitive-equation model with a free surface. Relaxation proceeds from the 15th day of each month, after the climatology-driven model has reached a steady annual cycle. The simulation clearly deviates from a realistic setting in which winds fluctuate with a wide range of spatial and temporal scales, but proves to be useful in identifying a likely generating mechanism for the winter appearance of a northeastward warm current. Winter northeasterly winds drive a southwestward coastal current along the northwestern boundary of the basin. This current piles up waters to the south. The return current after wind relaxes produces the northeastward warm current in the northwestern reaches of the basin. That the return surge is confined to the northwestern boundary of the basin suggests that continental shelf waves are primarily responsible. Although the northeastward warm current is bounded to the left by the coastline, disturbances triggered by relaxation events must propagate as continental shelf waves in the opposite direction.

The barotropic mechanism ensures a fast response of the northeastward warm current approximately at the right location and with the right alongshore span soon after the wind relaxes. Discrepancies remain and are mostly related to the lack of baroclinicity. The observed warm current extends deeper (300 m) into the water column and centers about deeper isobaths (200–400 m) than what has been suggested by the present model. Although the observed warm current attenuated slowly with depths, the vertical shear is nevertheless adequate to geostrophically deepen offshore isotherms. This baroclinic feature is mostly wanting in the present model. Observations also suggest that the maximum speed (~30 cm/s) and transport (≤10 Sv) of the South China Sea Warm Current are likely larger than model estimates. If wind relaxation is indeed the generating mechanism of the warm current in winter, some of the discrepancies can be explained by the unsteadiness of northeasterly winds, while others require some dynamical speculations. Each discrepancy is discussed below.

Our model wind fields are averaged over many years with one-degree resolution. The climatology-derived circulation prior to wind relaxation, as in all previous models, contains a reasonable Kuroshio intrusion current but not the South China Sea Warm Current in winter. The spatial and temporal averaging can easily lead to a two- or three-fold underestimate of real winds that fluctuate in time and space. Assuming that real northeasterly winds deviate from monthly averages by a series of sinusoidal components oscillating on weekly time scales, frequent and rapid decelerations of episodic wind events much stronger in strength than monthly averages may sustain a much swifter warm current. Each episode excites a barotropic current superimposed on the remnant of the last one. One can imagine how this initially barotropic current gradually transforms into a baroclinic current. If persistent and strong, the northeastward current will be able to carry a substantial amount of warm water from the south northeastward. The contrast between the warm water and ambient cold water, in turn, will suspend the current in the upper water column by geostrophy. The present model conceptualizes the generating mechanism by one wind relaxation event, through which the consequent northeastward current persists largely unattenuated only for about 15 days, not long enough to establish adequate baroclinicity. In this light, the desired baroclinic signature in the warm current is likely to require numerous episodes of wind relaxation, and the observed isotherm slope associated with this current may be an indication of its persistence, never steady in time but frequently occurring. The real warm current overlies somewhat deeper isobaths than does the modeled current. While the present model

resolution may be too coarse to rectify this modest discrepancy, intermittent northeasterly winds over longer time scales may displace the current somewhat offshore.

Inspite of discrepancies, wind relaxation stands out as a distinct possibility responsible for the generation of the South China Sea Warm Current in winter. Even in summer months, although the wind relaxation is not a necessary condition to trigger the northeastward warm current, our model suggests that the sea surface slope along the western boundary of the basin is able to sustain the warm current during occasional wind relaxations. To advance the hypothesis further, it would be necessary to drive the model ocean using realistic wind fields with sufficient temporal resolution, and to establish the persistence and characteristics of the warm current therefrom. There are technical difficulties to be overcome in such an endeavor. To extend the model's prognostic skill to below monthly time scales, it is not known how inflows and outflows through open boundaries fluctuate with wind fields over the South China Sea. Removing this uncertainty requires not only credible radiation conditions for barotropic components of currents on open boundaries, but also the knowledge of how much of inflow/outflow fluctuations are remotely driven by forcings outside the basin. These are the underlying difficulties preventing us from pursuing this subject further at this moment. Another possibility would be to analyze results from a global circulation model with sufficient temporal and spatial resolutions. Such a model has yet to be developed.

Acknowledgements

We are indebted to Sunny Y. Wu for her programming assistance, to N. Imasato who went beyond the duty of an editor to provide editorial comments, and to an anonymous reviewer for his thorough and constructive comments.

References

Buchwald, V. T. and J. K. Adams (1968): The propagation of continental shelf waves. *Proc. Roy. Soc. London*, **A305**, 235–250.

Guan, B. (1978): New evidences of the South China Sea Warm Current. *Ocean Sciences* (supplement), 100–103 (in Chinese).

Guan, B. (1985): Some features of the temporal and spatial distributions of the "counter-wind" current in northern South China Sea in winter. *Oceanologia et Limnologia Sinica*, **16**(6), 429–438 (in Chinese with English abstract).

Guo, Z. and Y. Huang (1983): Effects of the cold wave on the warm current in the South China Sea. *Tropic Oceanology*, **2**(2), 102–107 (in Chinese with English abstract).

Guo, Z., T. Yang and D. Qiu (1985): The South China Sea Warm Current and the southwestward current on its right side in winter. *Tropic Oceanology*, **4**(1), 1–9 (in Chinese with English abstract).

Hellerman, S. and M. Rosenstein (1983): Normal monthly wind stress over the world ocean with error estimates. *J. Phys. Oceanogr.*, **13**, 1093–1104.

Li, R., Z. Ji and Q. Zeng (1992): A numerical simulation of the western Pacific circulation. p. 115–126. In *Symposium of Ocean Circulation*. Ocean Press, Beijing (in Chinese).

Levitus, S. (1982): Climatological Atlas of the world ocean, NOAA Professional paper No. 13, U.S. Government Printing Office, Washington, D.C., 173 pp.

Pacanowski, R. C. and S. G. H. Philander (1981): Parameterization of vertical mixing in numerical models of tropical oceans. *J. Phys. Oceanogr.*, **11**, 1443–1451.

Pohlmann, T. (1987): A three dimensional circulation model of the South China Sea. p. 245–268. In *Three-Dimensional Models of Marine and Estuarine Dynamics*, ed. by J. J. Nihoul and B. M. Jamart, Elsevier, New York.

Shaw, P. T. (1989): The intrusion of water masses into the sea southwest of Taiwan. *J. Geophys. Res.*, **94**, 18213–18226.

Shaw, P. T. (1991): The seasonal variation of the intrusion of the Philippine Sea water into the South China Sea. *J. Geophys. Res.*, **96**, 821–827.

Shaw, P. T. and S. Y. Chao (1994): Surface circulation in the South China Sea. *Deep-Sea Res.* (in press).
Wyrtki, K. (1961): Physical Oceanography of the Southeast Asian Waters, NAGA Report Vol. 2, Scientific Results of Marine Investigations of the South China Sea and the Gulf of Thailand, Scripps Institution of Oceanography, La Jolla, Calif., 195 pp.
Zeng, Q., R. Li, Z. Ji, Z. Gan and P. Ke (1989): Calculations of the monthly mean circulation in the South China Sea. *Scientia Atmospherica Sinica*, **13**, 127–168 (in Chinese).